Synthesis, Crystal Structure, Magnetism, and Magnetic Anisotropy of Cyclic Clusters Comprising Six Iron(III) Ions and Entrapping Alkaline Ions

Andrea Caneschi, Andrea Cornia, Antonio C. Fabretti, Simon Foner, Dante Gatteschi,* Romano Grandi, and Luisa Schenetti

Abstract: The reaction of ferric chloride and β-diketones (HL) in alkaline methanol solution represents a good synthetic route to hexairon(III) clusters $[MFe_6(OCH_3)_{12}(L)_6]^+$ (M = Na, Li), which exhibit an unusual sixfold molecular symmetry. Single-crystal X-ray diffraction showed that the six octahedrally coordinated iron(III) ions define a ring and are linked by twelve bridging methoxide ligands. The resulting $[Fe_6(OCH_3)_{12}]$ skeleton has the remarkable property of acting as a host for an alkali-metal ion both in the solid state and in organic solution, as demonstrated by ^{23}Na and ^{7}Li NMR experiments. The magnetic behavior of these systems is consistent with the presence of a nonmagnetic $S = 0$ ground state and of antiferromagnetic exchange interactions between the high-spin ferric ions. The energy of the excited states was studied in detail by high-field DC and pulsed-field differential magnetization experiments at 0.7 and 1.5 K. Single-crystal susceptibility measurements at variable temperature revealed a sizeable magnetic anisotropy, which has been successfully analyzed in terms of single-ion and dipolar contributions. The results are relevant to research into the origin of superparamagnetic-type behavior in transition-metal clusters.

Keywords
aggregates · clusters · host guest chemistry · iron complexes · magnetic anisotropy

Introduction

Iron and manganese clusters have received much attention in recent years for several different reasons. When assembled by hydrolytic polymerization of low-nuclearity (often monomeric) precursors, they can contribute to an understanding of biomineralization processes in natural environments.[1] Synthetic models have provided considerable insight into the structural and functional properties of some metalloproteins,[2] and are often intrinsically attractive for their physical properties. In particular, large polyiron[3a] and polymanganese[3b-d] complexes are of interest for obtaining nanometer-sized magnetic particles with high-spin ground states. The latter feature, when combined with a large Ising-type magnetic anisotropy, may give rise to superparamagnetic-type behavior.[3c] Magnetic anisotropy in molecular clusters is therefore actively investigated, but a detailed analysis of the different anisotropic contributions (single-ion, dipolar, exchange) is often not possible owing to structural complexity.[4]

In an investigation of antiferromagnetic iron(III) alkoxide clusters, which provided a series of dinuclear,[5] trinuclear,[6] tetranuclear,[5] and decanuclear[7] complexes, we isolated hexairon(III) clusters with a cyclic structure and general formula $[MFe_6(OCH_3)_{12}(dbm)_6]^+$ (M = Na, Li).[8] The synthesis and solid-state structure of the complex $[NaFe_6(OCH_3)_{12}(dbm)_6]^+$ (**1**) has been communicated.[9] As an extension of this work, we present herein a detailed report of the synthesis, X-ray structure, and magnetism of **1**, and of the isostructural complex $[NaFe_6(OCH_3)_{12}(pmdbm)_6]^+$ (**2**).[8] The cation **2** in $[2](ClO_4)\cdot x CHCl_3 \cdot y CH_3OH$ has crystallographically imposed S_6 symmetry; single-crystal magnetic susceptibility measurements allowed a detailed study of the sources of molecular magnetic anisotropy. The model adopted for the interpretation of the magnetism of **1** and **2** is supported by the results of high-field magnetization measurements on **1**. In the context of a CdI_2-type structure, which is typical of the cores of several iron(III) alkoxo clusters, we present some spin topologies that are expected to have high-spin ground states and an Ising-type anisotropy while retaining antiferromagnetic spin–spin interactions.

Results

Synthesis and solution studies: The reaction of iron(III) chloride with 4 equiv of an alkali-metal methoxide ($MOCH_3$) and 1 equiv of β-diketone (HL = Hdbm, Hpmdbm, Hdpm)[8] in anhydrous methanol resulted in the precipitation of a yellow-to-red solid containing a 1:1 iron-to-L ratio. X-ray-quality crystals

[*] Prof. D. Gatteschi, Dr. A. Caneschi
Dipartimento di Chimica, Università degli Studi di Firenze
I-50144 Florence (Italy)
Fax: Int. code +(55)35-4845
e-mail: gattesch@chim1.unifi.it
Dr. A. Cornia, Prof. A. C. Fabretti, Prof. R. Grandi, Prof. L. Schenetti
Dipartimento di Chimica, Università degli Studi di Modena (Italy)
Prof. S. Foner
Francis Bitter National Magnet Laboratory, M. I. T.
Cambridge, MA 02139 (USA

  0947-6539/96/0211-1379 $ 15.00+.25/0

of the triiron(III) cluster $[KFe_3(OCH_3)_7(dbm)_3]\cdot 4CH_3OH$ ([3]·4CH$_3$OH) could be grown directly from the filtered reaction mixture.[6] More frequently, microcrystalline precipitates were obtained. They were quite soluble in moderately polar organic solvents ($CHCl_3$, CH_2Cl_2, $CH_3C_6H_5$) and, simply by adjustment of recrystallization techniques, could be used as starting materials for the synthesis of a wide series of iron(III) alkoxo complexes with general formula $[M_pFe_nO_m(OCH_3)_x(L)_yX_w]$ ($n = 2, 4, 6, 10$), where X is a mononegative ion (Cl^-, ClO_4^-).[5, 7, 9] In particular, slow evaporation of $CHCl_3$/CH_3OH solutions of the crude precipitate obtained with M = Na, Li and Hdbm afforded orange crystals of $[MFe_6(OCH_3)_{12}(dbm)_6]^+$ as chloride salts.[9] By using sodium methylate and Hpmdbm and carrying out recrystallization in the presence of sodium perchlorate, we isolated an analogous compound $[2](ClO_4)\cdot x CHCl_3\cdot y CH_3OH$ as large deep red hexagonal prisms (Scheme 1). The values of x and y are uncertain, since the crystals crack and lose weight when removed from the mother liquor. The vacuum-dried material was analyzed as $[NaFe_6(OCH_3)_{12}(pmdbm)_6](ClO_4)$, but the crystal density calculated on the basis of the above formula and of the unit cell volume (Table 1) is unreasonably low. Therefore, solvent molecules of crystallization may be present that are removed in vacuo. A somewhat analogous situation is encountered with compound [1](Cl)·CHCl$_3$·12CH$_3$OH[9] and is not uncommon in cluster chemistry.

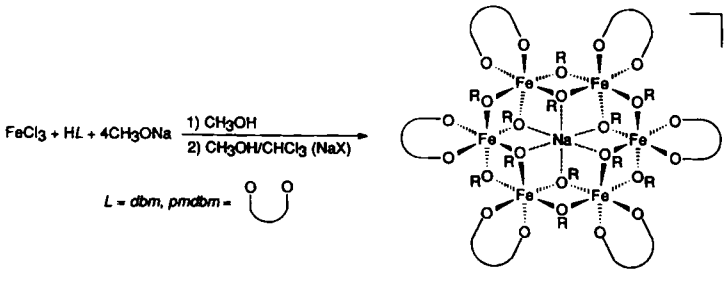

Scheme 1. Synthetic route to complexes **1** (L = dbm) and **2** (L = pmdbm) (R = CH$_3$).

Table 1. Crystallographic data for compound $[2](ClO_4)\cdot x CHCl_3\cdot y CH_3OH$.

chemical formula [a]	$C_{114}H_{126}Fe_6O_{40}NaCl$
formula weight [a]	2529.76
crystal system	trigonal
space group [b]	$R\bar{3}$
a (Å)	28.588(4)
c (Å)	16.211(4)
V (Å^3)	11475(3)
Z	3
ρ_{calcd} (g cm^{-3}) [a]	1.10
T (K)	298
radiation	$Mo_{K\alpha}$
λ (Å)	0.71069
μ (cm^{-1}) [a]	5.9
range of 2θ (°)	4.1–55.3
no. of collected reflns	6348
no. of unique reflns	4862
no. of reflns with $F_o^2 > 3\sigma(F_o^2)$	3159
no. of parameters	258
refl./param. ratio	12.2
$R(F_o)$ [c]	0.069
$R_w(F_o)$ [d]	0.075

[a] With $x = y = 0$. [b] Ref. [31]. [c] $R = \sum||F_o| - |F_c||/\sum|F_o|$. [d] $R_w = w^{1/2}||F_o| - |F_c||/\sum w^{1/2}|F_o|$ with $w = 1.0/[\sigma^2(F_o) + 1 \times 10^{-2}F_o^2]$.

^{23}Na NMR experiments were performed in order to test the stability of **1** in organic solution. A broad signal at $\delta \approx -30$ was detected in 3×10^{-2} M $CDCl_3$ solutions of [1](Cl)·$CHCl_3$·12CH_3OH (Fig. 1a). Upon addition of 1 equiv of sodium tetraphenylborate, an additional, narrower signal appeared at $\delta \approx 0$ (Fig. 1b). The two peaks, which clearly differ in chemical shift and band width, were assigned to encapsulated and free Na^+ ions, respectively. These observations clearly indicate that the exchange reaction of the encapsulated sodium ion with the bulk of the solution proceeds slowly on the NMR timescale and that cation **1** is fully associated in chloroform solution.[10]

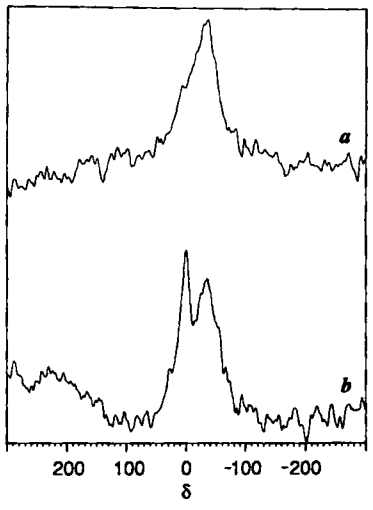

Fig. 1. a) Solution ^{23}Na spectrum of [1](Cl)·$CHCl_3$·12CH_3OH in $CDCl_3$; b) the same after the addition of 1 equiv of $NaBPh_4$. Chemical shifts are referenced to external NaCl (sat.) in $CDCl_3$.

Molecular structure: The crystal structure of $[2](ClO_4)\cdot x CHCl_3\cdot y CH_3OH$ comprises cationic hexanuclear units $[NaFe_6(OCH_3)_{12}(pmdbm)_6]^+$ (Fig. 2), perchlorate anions and crystallization solvent molecules ($CHCl_3$, CH_3OH). The latter must be highly disordered since they were not revealed by the X-ray analysis. The $[NaFe_6(OCH_3)_{12}(pmdbm)_6]^+$ (**2**) cation is isostructural with $[NaFe_6(OCH_3)_{12}(dbm)_6]^+$ (**1**),[9] though the crystallographic point-group symmetry of the two clusters is different (S_6 and C_i, respectively). Selected interatomic distances and angles for **1** and **2** are presented in Table 2.

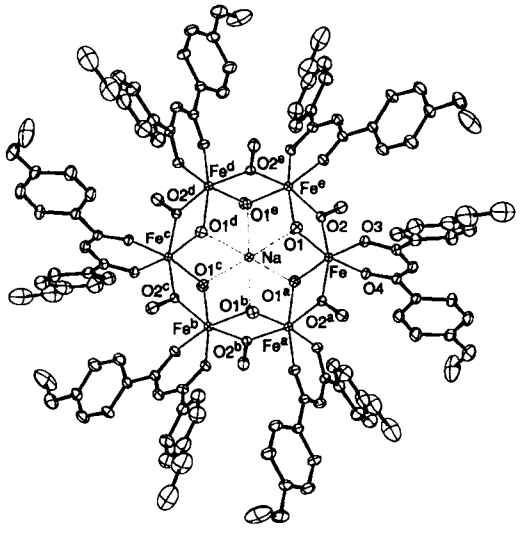

Fig. 2. Molecular structure of **2** at 298 K showing the atom labeling scheme (see footnote in Table 2). Thermal ellipsoids at 20% probability. Hydrogen atoms have been omitted for clarity.

The six crystallographically equivalent iron(III) ions in **2** are arranged at the vertices of an almost regular hexagon [Fe···Fe (min) 3.2152(5) Å, Fe···Fe^a···Fe^b 119.781(4)°] and lie essen-

0947-6539/96/0211-1380 $ 15.00+.25/0 Chem. Eur. J. 1996, 2, No. 11

Table 2. Interatomic distances (Å) and angles (°) in [1](Cl)·$CHCl_3$·$12CH_3OH$ and [2](ClO_4)·$x CHCl_3$·$y CH_3OH$ [a].

	1	2
Fe···Fe^a	3.184–3.201 (av. 3.195)	3.2152(5)
Fe···Fe^b	5.516–5.542 (av. 5.532)	5.5627(9)
Fe···Fe^c	6.366–6.413 (av. 6.39)	6.425(1)
Fe–O1	2.022–2.032 (av. 2.026)	2.023(3)
Fe–O1^a	2.019–2.029 (av. 2.025)	2.041(3)
Fe–O2	2.005–2.016 (av. 2.009)	2.000(4)
Fe–O2^a	2.001–2.003 (av. 2.002)	2.014(3)
Fe–O3	1.983–1.996 (av. 1.992)	2.001(3)
Fe–O4	1.975–1.979 (av. 1.977)	1.982(3)
Na–O1	2.338–2.374 (av. 2.351)	2.352(1)
Fe···Fe^a···Fe^b	119.51–120.52 (av. 120.0)	119.781(4)
O2-Fe-O1	74.7–75.5 (av. 75.0)	74.8(1)
O2^a-Fe-O1^a	75.1–75.5 (av. 75.2)	74.1(1)
O3-Fe-O1	89.2–90.1 (av. 89.6)	89.0(1)
O4-Fe-O1^a	92.5–93.0 (av. 92.7)	93.8(2)
O3-Fe-O2	99.6–102.6 (av. 100.7)	101.6(2)
O4-Fe-O2	89.7–92.5 (av. 91.3)	94.4(1)
O4-Fe-O3	85.9–86.9 (av. 86.5)	85.8(1)
O2^a-Fe-O1	94.7–95.4 (av. 95.0)	97.2(2)
O2-Fe-O1^a	92.7–93.1 (av. 92.9)	90.9(1)
O3-Fe-O2^a	89.9–92.5 (av. 91.6)	93.4(2)
O4-Fe-O2^a	98.4–101.3 (av. 99.8)	95.2(2)
O1-Fe-O1^a	94.3–95.0 (av. 94.6)	93.8(2)
O4-Fe-O1	163.0–166.3 (av. 164.8)	166.8(1)
O3-Fe-O1^a	164.6–167.7 (av. 166.5)	167.4(1)
O2-Fe-O2^a	163.8–164.2 (av. 164.0)	162.7(2)
O1-Na-O1^a	78.6–78.8 (av. 78.7)	78.2(1)
O1-Na-O1^b	101.2–101.8 (av. 101.5)	101.8(1)
Fe-O1^a-Fe^a	103.7–104.4 (av. 104.1)	104.6(2)
Fe-O2^a-Fe^a	105.3–105.8 (av. 105.6)	106.5(2)

[a] Superscripts are used for symmetry-equivalent atoms ($X^a = S_6^1(X)$, $X^b = S_6^2(X)$, $X^c = S_6^3(X)$, etc.).

tially on a plane (deviation: 0.076 Å). The coordination spheres of the metals are exclusively occupied by oxygen donors. Twelve methoxide ions act as bridges between adjacent iron(III) centers and support the cyclic skeleton of the cluster, which approaches D_{3d} symmetry. Each metal ion is further coordinated by a chelating pmdbm ligand. The octahedral coordination geometry of the iron(III) ions is considerably distorted (Fig. 3) as a consequence of the constraints imposed by the double methoxide bridges and by the bite angle of the pmdbm ligand. In particular the angles O1-Fe-O2 and O1^a-Fe-O2^a are remarkably acute [74.8(1) and 74.1(1)°, respectively] compared with the octahedral value and with the (CH_3)O-Fe-O(CH_3) angle in the dimer $[Fe_2(OCH_3)_2$-$(dbm)_4]$ [80.0(2)°].[5]

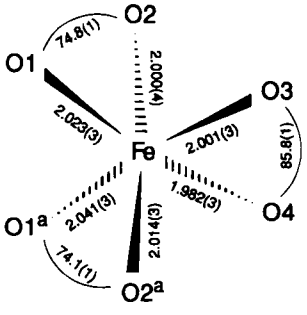

Fig. 3. Schematic representation of the coordination sphere of the metal ions in **2**. The values of selected bond lengths (Å) and angles (°) are indicated.

The two methoxide ligands of each $Fe_2(OCH_3)_2$ unit lie on opposite sides of the average plane through the metals and at different distances from the molecular $\bar{3}$ axis. Six OCH_3 ligands that are closer to the unique axis have their O–C bond almost perpendicular to the molecular plane (85.6°); the O–C vectors of the remaining methoxides form a remarkably acute angle with the plane through the metals (49.0°). The special position of $\bar{3}$ symmetry in the middle of the cluster is occupied by the sodium ion, which is coordinated by methoxide ligands of the first subset (O1, O1^a, O1^b, etc.). As a consequence of the interaction with the sodium ion, the Fe–O1 and Fe–O1^a distances are slightly elongated with respect to Fe–O2 and Fe–O2^a (Table 2).

Magnetism: The magnetic susceptibility of a vacuum-dried sample of polycrystalline powder of [2](ClO_4)·$x CHCl_3$·$y CH_3OH$ measured at 1 T is shown in Figure 4 as a function of temperature. A broad maximum is detected at about 150 K,

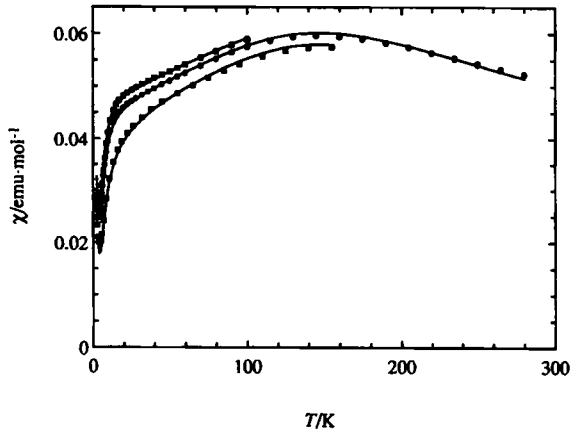

Fig. 4. Magnetic susceptibility of [2](ClO_4)·$x CHCl_3$·$y CH_3OH$ at 1 T as a function of temperature. ● represent powder data, whereas $\chi_\parallel$ and $\chi_\perp$ are represented by ■ (lower trace) and □ (upper trace), respectively. Solid lines are calculated susceptibilities with $j'_{eff} = 13.69\ cm^{-1}$, $g = 2.00$, $D_a = D_{ab} = 0$, $p = 1.7\%$ (powder data) or with $j'_{eff} = 13.69\ cm^{-1}$, $g_\parallel = 1.965$, $g_\perp = 2.020$, $D_a = -0.050\ cm^{-1}$, $D_{ab} = 0.055\ cm^{-1}$, $p = 1.4\%$ (single-crystal data).

which is typical of antiferromagnetically coupled systems with an $S = 0$ ground state. The χT product decreases from 14.62 emu K mol^{-1} at 280 K to 0.067 emu K mol^{-1} at 2.3 K. For comparison, the calculated value for six uncoupled $S = 5/2$ spins with $g = 2.00$ is 26.26 emu K mol^{-1}. The isostructural complex **1** shows identical behavior.[9] However, the uniaxial symmetry of the crystals of [2](ClO_4)·$x CHCl_3$·$y CH_3OH$ permitted magnetic susceptibility measurements with the magnetic field either parallel or perpendicular to the molecular $\bar{3}$ axis. The temperature dependence of $\chi_\parallel$ and $\chi_\perp$ at 1 T was experimentally determined over the temperature ranges 2.2–150 K and 2.2–100 K, respectively, as shown in Figure 4. Quite a large magnetic anisotropy was detected, with $\chi_\parallel < \chi_\perp$. While $\chi_\parallel$ decreased fairly smoothly on cooling the sample, $\chi_\perp$ decreased almost linearly in the range 100–15 K and then underwent an abrupt decrease.

The results of high-field DC magnetization measurements on a powdered sample of [1](Cl)·$CHCl_3$·$12CH_3OH$ at 0.7 K and 1.5 K are shown in Figure 5. The magnetization was essentially zero at low fields, as expected for a nonmagnetic ground state for **1**. Close examination of the 0.7 K data shows a slightly negative magnetization at low fields because of contributions of the addenda and the powder matrix diamagnetism; at 1.5 K evidence of a slightly increased population of higher states is seen in that field range. The start of the first step in the magnetization due to level crossing was observed above about 11 T and was completed by about 20 T. The step for both sets of data occurred at about 16.4 T, corresponding to the inflection points. The width of the step (5.1 and 3.2 T at 1.5 and 0.7 K, respective-

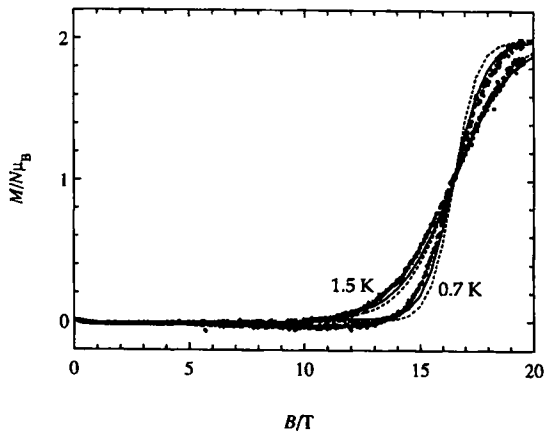

Fig. 5. Plot of reduced magnetization of [1](Cl)·$CHCl_3$·12CH_3OH measured at 0.7 and 1.5 K with increasing field (•), and calculated powder averages at the same temperatures (solid lines: $j_{eff} = 15.4\ cm^{-1}$, $g = 2.00$, $D_a = -0.050\ cm^{-1}$, $D_{ab} = 0.055\ cm^{-1}$, $p = 0$; broken lines: $j_{eff} = 15.4\ cm^{-1}$, $g = 2.00$, $D_a = D_{ab} = 0$, $p = 0$).

ly) was less at the lower temperature, though it did not scale as would be expected for only thermal broadening of the step. The data were extended to higher fields with pulsed field differential magnetization measurements at 1.5 K, as discussed in ref. [11]. The data up to 52 T (Fig. 6) showed the first 3 of 15 steps expect-

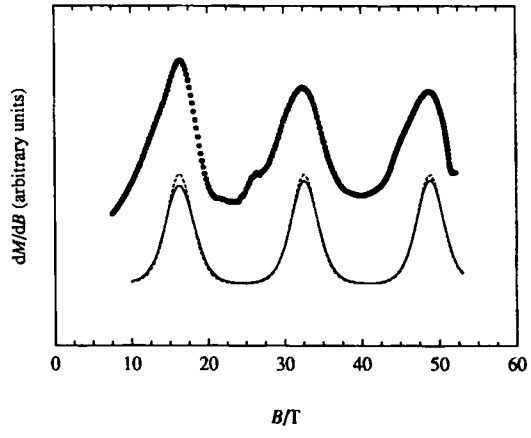

Fig. 6. Plot of differential magnetization of [1](Cl)·$CHCl_3$·12CH_3OH measured at 1.5 K with decreasing field (•), and calculated powder averages at the same temperature (solid line: $j_{eff} = 15.2\ cm^{-1}$, $g = 2.00$, $D_a = -0.050\ cm^{-1}$, $D_{ab} = 0.055\ cm^{-1}$, $p = 0$; broken line: $j_{eff} = 15.2\ cm^{-1}$, $g = 2.00$, $D_a = D_{ab} = 0$, $p = 0$).

ed for **1**. The maxima of dM/dB were sited at 16.4, 32.4, and 48.8 T. The position of the first step is in good agreement with DC data. The step width at half maximum is the same (≈ 6 T) for each of the three steps.

Discussion

Synthesis and solution studies: The use of alkali-metal alkoxides represents a convenient strategy for assembling polynuclear iron compounds,[12] although precise structural information on iron(III) alkoxide clusters has only recently been obtained by X-ray investigations.[5-7, 9, 13-15] The use of alkoxide-promoted processes has a major advantage with respect to hydrolytic reactions: the formation of alkoxo-bridged polynuclear complexes is easier to control owing to the inability of the RO^- ligand to coordinate more than three metal atoms. However, alcoholysis and hydrolysis are in general competing reactions in synthetic media, as was demonstrated by the isolation of iron (III) clusters with mixed alkoxide and oxide ligands.[7, 14a-c] Hydrolytic polymerization of solid iron alkoxide complexes occurs rapidly upon prolonged exposure to wet air and leads to the formation of insoluble rusty materials.[13] Similar reactions in solution have found a practical application in the deposition of thin layers of iron oxides with the sol-gel technique.[16]

Since the binding properties of alkoxides are not dissimilar to those of hydroxide ligands, the isolation of **1** and **2** suggests that cyclic hexairon clusters may be important intermediates in iron aggregation processes promoted by hydroxides. A cyclic structure has previously been postulated for hexanuclear species with the tentative formula $[Fe_6(OH)_{12}(sor)_6]^{6+}$[8] that form in aqueous solutions of iron(III) and sorbitol and lead to gels at neutral pH.[17] The sorbitol molecule would chelate the metal ions. In more alkaline media, dimeric and monomeric complexes are believed to exist that bear direct structural resemblance to dialkoxo-bridged $[Fe_2(OCH_3)_2(L)_4]$[5] and mononuclear $[Fe(L)_3]$. The presence of an encapsulated Na^+ ion in **1** and **2**, discovered in the solid state and confirmed in $CDCl_3$ solution by NMR techniques, suggests that the structurally similar cores of hydroxo-bridged clusters may have analogous host properties. The cyclic $[Fe_6(OCH_3)_{12}(L)_6]$ moiety of **1** and **2** has marked hydrophobic characteristics caused by the bulky shell of organic residues on L ligands and easily solubilizes alkali-metal ions in moderately polar organic solvents. Though more detailed solution studies are in progress, the analogy between **1** and **2** and crown-ether metal complexes is apparent.[9, 18]

Solid-state structure: Polynuclear compounds with a cyclic structure are by no means rare in transition-metal chemistry.[9] Recently, hexanuclear complexes of cyclohexasiloxanolates with first-row transition metal ions have been reported.[19] Iron(II) ring complexes with sulfur ligands have also been isolated.[9] In contrast, only two cyclic iron(III) clusters have previously been studied, namely $[NaFe_6O_4(OH)_2(ami)_4(phen)_8](NO_3)_9 \cdot 10H_2O$ (**4**)[8, 20] and $[Fe_{10}(OCH_3)_{20}(CH_2ClCO_2)_{10}]$ (**5**).[13] The $Fe_6(\mu_2\text{-}O)_4(\mu_2\text{-}OH)_2(\mu_2\text{-}O_2CR)_4$ core of **4** has a much lower symmetry than **1** and **2**. Decairon(III) complex **5** is structurally similar to **1** and **2**. Its $Fe_{10}(OCH_3)_{20}$ skeleton is supported by double methoxide bridges and has an idealized D_{5d} symmetry. The coordination geometry of the iron(III) ions in **5** is also very similar to that encountered in **1** and **2**. However, one main feature distinguishes the core of **1** and **2** from that of **5**: the oxygen atoms in **1** and **2** are arranged in two parallel c.p. layers, each one comprising twelve atoms (1st layer: O1, O3, $O2^a$, $O4^a$, $O1^b$, $O3^b$, etc.; 2nd layer: O2, O4, $O1^a$, $O3^a$, $O2^b$, $O4^b$, etc.; av. dev. 0.145 Å). The metal ions (Fe^{3+} and Na^+) are found in the octahedral interstices, and the topology of the core is that of a CdI_2-type lattice (Fig. 7). This feature is often observed in iron(III) hydroxo and alkoxo clusters and recalls the solid-state structures of iron oxides and hydroxides,[6] which are the final products of hydrolysis of iron salts. In particular, the central Fe_7 moiety of two remarkable clusters recently isolated from aqueous environments (Fe_{17} and Fe_{19})[21] can be formally constructed from the core of **1** and **2** by substituting the encapsulated Na^+ ion with a Fe^{3+} ion. Without the central sodium ion, the cyclic structure of **1** and **2** is also directly analogous to that of gibbsite $[Al(OH)_3]$.

Magnetism: Cyclic polynuclear complexes are magnetically attractive as models for infinite one-dimensional compounds and have been extensively investigated in the past.[22] Furthermore,

0947-6539/96/0211-1382 $ 15.00+.25/0 Chem. Eur. J. 1996, 2, No. 11

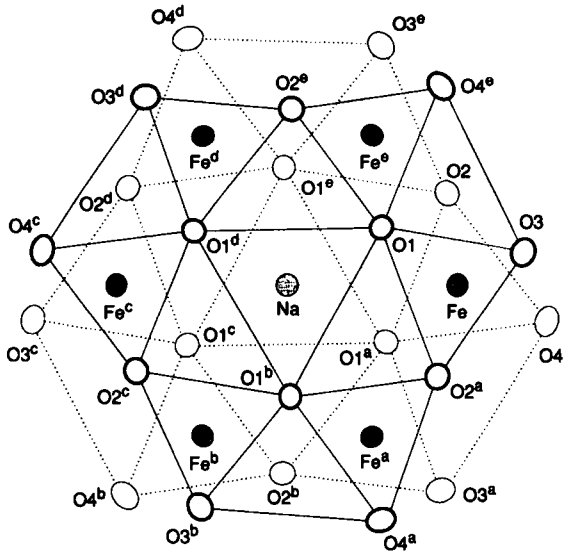

Fig. 7. Structure of the iron–oxygen core of **2** (see footnote in Table 2). Solid and dotted lines connect the oxygen atoms belonging to the upper and lower layers, respectively.

they often exhibit high molecular symmetries, which considerably simplify theoretical treatments. For a cluster of six $S_i = 5/2$ spins there are $6^6 = 46{,}656$ states that must be included in the calculation of the energy levels and of the magnetic susceptibility by the standard Heisenberg hamiltonian (1), which describes

$$\mathcal{H} = J\sum_{i=1}^{5} \boldsymbol{S}_i\cdot\boldsymbol{S}_{i+1} + J\boldsymbol{S}_6\cdot\boldsymbol{S}_1 \qquad (1)$$

nearest-neighbor interactions and assumes sixfold symmetry. The size of the matrices can be reduced by means of the symmetry properties of the total spin operator $\boldsymbol{S} = \sum_i \boldsymbol{S}_i$. In this way sixteen matrices, with size ranging from 1×1 to 609×609 and S values ranging from 15 to 0 must be calculated and diagonalized. This can be done very effectively with irreducible tensor operator techniques.[23]

The temperature dependence of the powder magnetic susceptibility of **2** clearly shows that the iron(III) ions are antiferromagnetically coupled and that the ground state has $S = 0$ (Fig. 4). A fit of the magnetic data provided $J = 19.89(3)\ \mathrm{cm}^{-1}$ for $g = 2.00$. This value compares well with those reported for similar alkoxo-bridged iron(III) clusters.[24] The low-temperature behavior was attributed to the presence of a mole fraction $p = 1.71(2)\%$ of a paramagnetic $S = 5/2$ impurity, which was assumed to follow a Curie-type law and to have a molecular weight equal to one sixth of that of the cluster.

More physical insight into the energy levels can be obtained through a simplified model that we have recently developed for the interpretation of magnetic data of antiferromagnetic rings comprising $2N$ symmetry-equivalent spins $\mathbf{S}_i$ with large S_i. As extensively described elsewhere,[25] this approach allows a straightforward treatment of magnetic anisotropy. A similar approach has been in part used by Gatteschi et al. for the interpretation of the low-temperature magnetization data of **5**.[13] However, in that case attention was focused on a small number of exchange multiplets; anisotropic contributions were neglected. The spins in the ring are partitioned into two sets, the ones which occupy odd and even sites, yielding resulting spins $\boldsymbol{S}_a$ and $\boldsymbol{S}_b$, defined in Equations (2a–b). The spin hamiltonian is then

$$\boldsymbol{S}_a = \boldsymbol{S}_1 + \boldsymbol{S}_3 + \boldsymbol{S}_5 + \ldots + \boldsymbol{S}_{2N-1} \qquad (2a)$$

$$\boldsymbol{S}_b = \boldsymbol{S}_2 + \boldsymbol{S}_4 + \boldsymbol{S}_6 + \ldots + \boldsymbol{S}_{2N} \qquad (2b)$$

written as a function of the $\boldsymbol{S}_a$ and $\boldsymbol{S}_b$ operators rather than of those associated with the individual spins $\boldsymbol{S}_i$. In this way it is simple to add low-symmetry components in order to take into account the anisotropy and the external magnetic field $\boldsymbol{B}$ [Eq. (3)]. The quantities j'_{eff} and j''_{eff} in Equation (3) are

$$\mathcal{H}_{eff} = j'_{eff}\boldsymbol{S}_a\cdot\boldsymbol{S}_b + \frac{j''_{eff}}{2}(\boldsymbol{S}_a^2 + \boldsymbol{S}_b^2) + \boldsymbol{S}_a\cdot\boldsymbol{D}_a(\alpha S_a)\cdot\boldsymbol{S}_a + \boldsymbol{S}_b\cdot\boldsymbol{D}_b(\alpha S_b)\cdot\boldsymbol{S}_b + \boldsymbol{S}_a\cdot\boldsymbol{D}_{ab}(\alpha S_a S_b)\cdot\boldsymbol{S}_b + \mu_B\boldsymbol{g}\cdot\boldsymbol{S}\cdot\boldsymbol{B} \qquad (3)$$

proportional to the true iron–iron coupling constant J. For $N = 3$ and $S_i = 5/2$, it can be shown that $j'_{eff} \approx 0.689J$ and $j''_{eff} \approx 0.072J$.[25] The $\boldsymbol{D}_a(\alpha S_a)$, $\boldsymbol{D}_b(\alpha S_b)$, and $\boldsymbol{D}_{ab}(\alpha S_a S_b)$ tensors, which will be assumed to be axial, describe anisotropic contributions and are functions of α, S_a, and S_b, where α stands for intermediate quantum numbers S_{13} and S_{24} ($\boldsymbol{S}_{ij} = \boldsymbol{S}_i + \boldsymbol{S}_j$). The physical meaning of Equation (3) is best appreciated by considering the isotropic term first. Since $j'_{eff} \gg j''_{eff}$, the states with the lowest energy arise from $S_a = S_b = 15/2$, that is, from a configuration in which "odd" spins are "up" and "even" spins are "down"; their energies follow Lande's rule [Eq. (4)], where S

$$E(S) = \frac{j'_{eff}}{2}S(S+1) \qquad (4)$$

ranges from 15 to 0 and the energy of the ground $S = 0$ state has been set to zero. Similar expressions hold for the excited configurations with $S_a = 13/2$, $S_b = 15/2$, $S_a = 13/2$, $S_b = 13/2$, etc. By neglecting anisotropic terms in Equation (3), it is possible to obtain an estimate for j'_{eff} from powder susceptibility data (Fig. 4). Setting $g = 2.00$, the best fit was achieved with $p = 1.70(2)\%$ and $j'_{eff} = 13.69(2)\ \mathrm{cm}^{-1}$, which corresponds to $J = 19.9\ \mathrm{cm}^{-1}$. This value is in complete agreement with that resulting from the application of hamiltonian (1).

We now turn to an interpretation of magnetic anisotropy as revealed by single-crystal measurements. For simplicity, we shall retain anisotropic contributions for the configurations $S_a = S_b = 15/2$ and $S_a = 13/2$, $S_b = 15/2$ only, which provide the main contribution to magnetic susceptibility in the temperature range examined. We shall further assume that $\boldsymbol{D}_a\left(5\frac{15}{2}\right) = \boldsymbol{D}_a\left(4\frac{13}{2}\right) = \boldsymbol{D}_a\left(5\frac{13}{2}\right) = \boldsymbol{D}_a$ and that $\boldsymbol{D}_{ab}\left(55\frac{15}{2}\frac{15}{2}\right) = \boldsymbol{D}_{ab}\left(45\frac{13}{2}\frac{15}{2}\right) = \boldsymbol{D}_{ab}\left(55\frac{13}{2}\frac{15}{2}\right) = \boldsymbol{D}_{ab}$. In the strong exchange limit, that is, when the first term in Equation (3) is dominant, the tensors $\boldsymbol{D}_k\left(5\frac{15}{2}\right)$ and $\boldsymbol{D}_{ab}\left(55\frac{15}{2}\frac{15}{2}\right)$ can be expressed as linear combinations of one-center (single-ion) and two-center (dipolar, anisotropic exchange) contributions[4, 25] [Eqs. (5) and (6)],

$$\boldsymbol{D}_k\left(5\frac{15}{2}\right) = \frac{2}{21}\sum_{i\in k}\boldsymbol{D}_i + \frac{5}{42}\sum_{ij\in k}\boldsymbol{D}_{ij} \qquad (5)$$

$$\boldsymbol{D}_{ab}\left(5\frac{15}{2}\frac{15}{2}\right) = \frac{1}{9}\sum_{i\in a,\,j\in b}\boldsymbol{D}_{ij} \qquad (6)$$

where i and j denote spin centers and $k = a, b$. Two-center contributions can be safely assumed to be essentially dipolar for $S_i = 5/2$ spins, and Equation 6 can be used to obtain an estimate for $\boldsymbol{D}_{ab}$. Since the principal axes of $\boldsymbol{D}_{ij}$ lie along $\boldsymbol{S}_i - \boldsymbol{S}_j$, which is essentially perpendicular to Z for the observed molecular

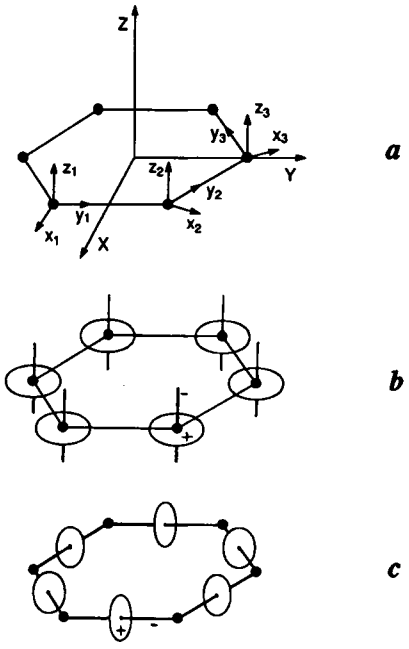

Fig. 8. Suggested orientations of single-ion zero-field splitting (*b*) and nearest-neighbor dipolar (*c*) tensors. The adopted local ($x_i y_i z_i$) and molecular (XYZ) reference frames are shown in (*a*).

geometry (Fig. 8a), the very simple relationships between zero-field splitting parameters described in Equations (7) and (8)

$$D_{ab} = -\frac{1}{3}D_{12} - \frac{1}{6}D_{14} \tag{7}$$

$$D_k = \frac{1}{7}D_1(3\cos^2\beta - 1) - \frac{5}{28}D_{13} \tag{8}$$

result, where β is the angle between Z and the principal axis of $\boldsymbol{D}_1$. For the experimental Fe–Fe separations and isotropic single-ion $\mathbf{g}_i$ tensors, $D_{12} = -0.156\ \mathrm{cm}^{-1}$, $D_{13} = -0.030\ \mathrm{cm}^{-1}$, $D_{14} = -0.019\ \mathrm{cm}^{-1}$, and Equation (7) yields $D_{ab} = 0.055\ \mathrm{cm}^{-1}$. A systematic sampling of the space of the variables D_a ($= D_b$), $g_\parallel$, and $g_\perp$ with $j'_{eff} = 13.69\ \mathrm{cm}^{-1}$, $\frac{j'_{eff}}{j''_{eff}} = 9.6$, and $D_{ab} = 0.055\ \mathrm{cm}^{-1}$ showed that the observed anisotropy can be accounted for by $D_a = -0.05\ \mathrm{cm}^{-1}$. In any case a good fit of the magnetic data at the highest measured temperatures requires a small anisotropy in the molecular g tensor. Representative curves are shown in Figure 4.

In order to obtain an estimate for D_i, β is required [Eq. (8)]. The values $D_i = -0.2\ \mathrm{cm}^{-1}$ and $D_i = 0.4\ \mathrm{cm}^{-1}$ result for $\beta = 0$ and 90°, respectively, that is, for the limiting cases in which the principal axis of $\boldsymbol{D}_1$ is parallel and perpendicular to Z, respectively. On the basis of the coordination geometry of the iron(III) ions and of the value $D_i = -0.11\ \mathrm{cm}^{-1}$ reported for Fe(acac)$_3$,[26] the former possibility seems the more reasonable and is consistent with recent findings on related iron(III) clusters.[27] The energy of the lowest-lying spin states for the suggested set of parameters is shown in Figure 9. The energy separation between the $m_s = 0$ and the $m_s = \pm 1$ states of the $S = 1$ multiplet is as large as 4 cm^{-1}. This is essentially due to the collinearity of the $\boldsymbol{D}_a$, $\boldsymbol{D}_b$, and $\boldsymbol{D}_{ab}$ tensors, to the opposite signs of D_k and D_{ab}, and to the large values of S_a and S_b. In the strong-exchange regime it can be shown that the $\boldsymbol{D}(S)$ tensors that describe the fine structure of the S states arising from the configuration

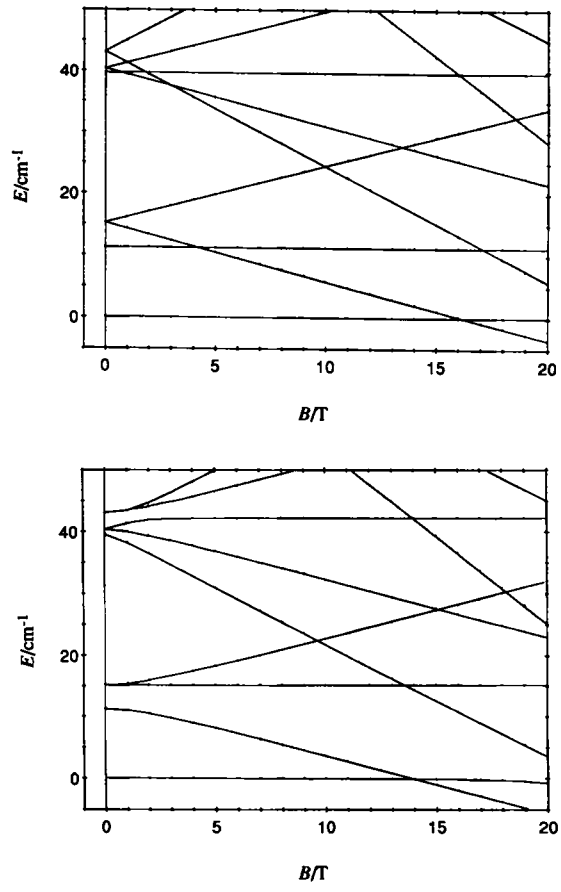

Fig. 9. Calculated energies of the lowest-lying spin states of **2** with $\boldsymbol{B} \parallel \bar{3}$ (top) and $\boldsymbol{B} \perp \bar{3}$ (bottom) for $j'_{eff} = 13.69\ \mathrm{cm}^{-1}$, $g_\parallel = 1.965$, $g_\perp = 2.020$, $D_a = -0.050\ \mathrm{cm}^{-1}$, and $D_{ab} = 0.055\ \mathrm{cm}^{-1}$.

$S_a = S_b = 15/2$ are given by Equation (9) [$d(S)$ is defined by Eq. (10)]. Since the $\boldsymbol{D}_a$, $\boldsymbol{D}_b$, and $\boldsymbol{D}_{ab}$ tensors have axial symmetry along Z, we may focus on the ZZ-components only. The axial single-ion zero-field splitting tensors $\boldsymbol{D}_i$, whose orientation is shown in Figure 8b, have *negative* components along Z, whereas dipolar tensors $\boldsymbol{D}_{i,i+1}$ (Fig. 8c) have *positive* components along the same axis. However, the two sets of components are projected with opposite signs on the S states and the ZZ-component of the tensor $[\boldsymbol{D}_a + \boldsymbol{D}_b - \boldsymbol{D}_{ab}]$ is *negative*. $d(S)$ is also large and negative for the states with a low S value, which therefore undergo *large positive* zero-field splittings.

$$\boldsymbol{D}(S) = d(S)[\boldsymbol{D}_a + \boldsymbol{D}_b - \boldsymbol{D}_{ab}] + {}^1/_2\boldsymbol{D}_{ab} \tag{9}$$

$$d(S) = \frac{3S(S+1) - 258}{2(2S+3)(2S-1)} \tag{10}$$

The step-like behavior of M as a function of B observed in both DC and pulsed-field magnetization measurements of **1** (Fig. 5 and 6) can be rationalized within the same model, since the ground state of the cluster is markedly field-dependent. If we neglect anisotropic terms in Equation (3), and label the states as $|\alpha S_a S_b S m\rangle$, the first step corresponds to the crossover from $\left|55\frac{15}{2}\frac{15}{2}00\right\rangle$ to $\left|55\frac{15}{2}\frac{15}{2}1-1\right\rangle$, the second to the crossover from $\left|55\frac{15}{2}\frac{15}{2}1-1\right\rangle$ to $\left|55\frac{15}{2}\frac{15}{2}2-2\right\rangle$, and so on (Fig. 10). Furthermore, since the energies of the lowest-lying exchange multiplets obey Lande's rule [Eq. (4)], the steps must occur at

0947-6539/96/0211-1384 $ 15.00+.25/0 Chem. Eur. J. 1996, 2, No. 11

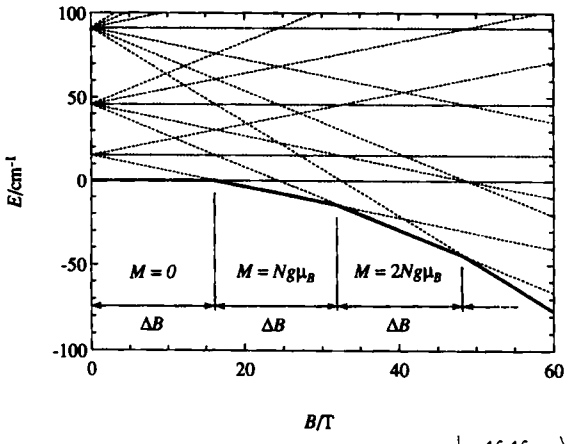

Fig. 10. Field dependence of the energy of the spin states $\left|55\frac{15}{2}\frac{15}{2}Sm\right\rangle$ for $S = 0$, 1, 2, and 3, calculated from hamiltonian (3) with $j'_{eff} = 15.2\ cm^{-1}$, $g = 2.00$, and $D_a = D_{ab} = 0$. The energy of the state $\left|55\frac{15}{2}\frac{15}{2}00\right\rangle$ has been set to zero. The expected saturation magnetization in each field interval is also reported.

regular field intervals, in good agreement with pulsed-field data. The spacing of the steps ΔB is related to j'_{eff} by Equation (11),[13] which allows the independent determination

$$\Delta B = \frac{j'_{eff}}{g\mu_B} \qquad (11)$$

of J. Assuming $g = 2.00$, the average spacing $\langle \Delta B \rangle = 16.3$ T leads to $j'_{eff} = 15.2\ cm^{-1}$ and $J = 22\ cm^{-1}$. These values are to be compared with $j'_{eff} = 13.69\ cm^{-1}$ and $J = 19.9\ cm^{-1}$ resulting from a fitting of the susceptibility of **2** in the temperature range 2.3–280 K. The calculated dM/dB versus B curve is reported in Figure 6 as a dashed line.

Magnetic anisotropy is expected to cause a broadening and possibly a shift of the steps, because the fields at which the crossovers take place become orientation-dependent (Fig. 9). However, a calculation performed with $j'_{eff} = 15.2\ cm^{-1}$, $g = 2.00$, $D_a = -0.050\ cm^{-1}$ and $D_{ab} = 0.055\ cm^{-1}$ (solid line in Fig. 6) shows that the positions of the steps at 1.5 K remain largely unaffected. The amount of anisotropy estimated from single-crystal susceptibility measurements is therefore perfectly consistent with the occurrence of equally spaced steps in the magnetization. Though the introduction of anisotropy causes some broadening of the steps, leading to a reasonable reproduction of DC data (Fig. 5), the width of the steps in a pulsed field is still largely unaccounted for. In contrast, the earlier dM/dB measurements made with **5**[13] showed narrowing of the steps in pulsed fields (9 were observed at 0.6 K for fields up to 45 T) as well as an increase of the step width with B. Furthermore, the steps in the DC data at 0.6 K were much narrower than for **1**.

In order to obtain an independent measurement of the zero-field splitting parameters, preliminary EPR experiments at 245 GHz were performed on a microcrystalline sample of **[2]**$(ClO_4)\cdot x CHCl_3 \cdot y CH_3OH$. However, no signal attributable to transitions within the first excited multiplets was detected in the temperature range 5–50 K.

Conclusions

Controlled methanolysis reactions have been used to assemble hexairon(III) complexes with an unprecedented sixfold molecular symmetry. Their cyclic skeleton is supported by double methoxide bridges and has the remarkable property of acting as a host for alkali-metal ions both in the solid state and in organic solution. The trigonally distorted coordination geometry of the metal ions and the essentially planar arrangement of the latter result in appreciable magnetic anisotropy. A reasonable estimate of single-ion anisotropy ($D_i = -0.2\ cm^{-1}$) has been obtained by application of a simplified spin-hamiltonian treatment that fully exploits the axial symmetry of the core and allows a straightforward treatment of magnetic anisotropy. Indeed, this is the first attempt to estimate the magnetic anisotropy in large iron(III) clusters that have nonmagnetic ground states. It is relevant that the anisotropy can be sizeable, thus creating the possibility of observing slow relaxation effects at low temperatures. However, the origin of the anisotropy can be explained on the basis of single-ion contributions and no need emerges for shape anisotropy effects. The interpretation of the superparamagnetic-type behavior observed in some iron(III) oxo clusters that we recently suggested is therefore supported.[27]

The topology of the oxygen and metal atoms in **1** and **2** is not uncommon. The core of several iron(III) clusters with methoxide and β-diketonate ligands can be described as a fragment of an extended layer with a CdI_2-type structure.[5–7] OCH_3 ligands often act as μ_2-species and mediate antiferromagnetic interactions. The coordination geometry of the metal ions is similar to that observed in **1** and **2**, and the principal axes of the single-ion zero-field splitting tensors are expected to be roughly perpendicular to the plane of the layer. On the basis of our estimate of D_i for **2**, it is now possible to envisage some antiferromagnetic systems with both a large value of S in the ground state and Ising-type anisotropy. We will restrict our analysis to molecular clusters with axial symmetry fitting the CdI_2 structure. The simplest case is that of a tetranuclear cluster **6** with a propeller-like structure (Fig. 11 a). Antiferromagnetic interactions are expected to lead to an $S = 5$ ground state in which the outer spin vectors are "up" and the inner is "down". Extension of the tetranuclear fragment in the plane of the layer while retaining threefold symmetry may lead to an Fe_{10} species **7** (Fig. 11 b).

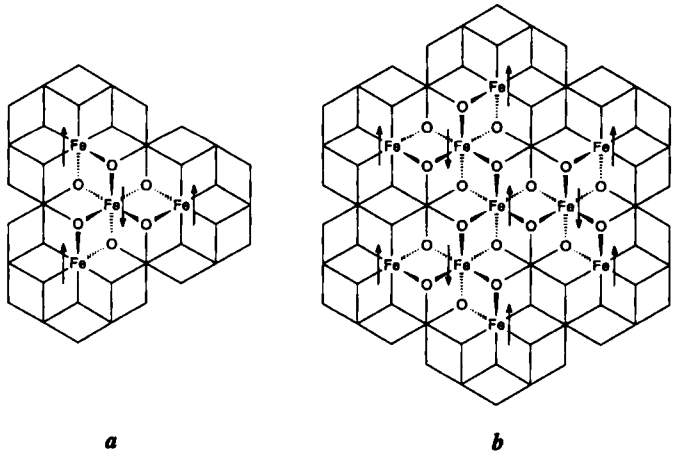

Fig. 11. Structure of compounds **6** (*a*) and **7** (*b*). See text for details.

The ground state is predicted to have $S = 10$, as a result of seven spins being "up" and three spins being "down". Assuming $D_i = -0.20\ cm^{-1}$ and the same nearest-neighbor Fe–Fe separation as in **2**, one obtains $D(5) = -0.17$ and $D(10) = -0.12\ cm^{-1}$ for **6** and **7**, respectively, at the strong-exchange limit.

Very recently, we isolated a cluster with structure **6** and an $S = 5$ ground state, namely $[Fe_4(OCH_3)_6(dpm)_6]$.[8] As will be extensively illustrated in a future report, the fine structure of the ground state has been dramatically revealed by low-temperature HF-EPR spectra, which showed that $D(5) = -0.20\ cm^{-1}$, in excellent agreement with our rough estimate.

Experimental Procedure

General methods: All operations were carried out under the exclusion of moisture, unless otherwise stated. Dimethoxyethane (DME, Acros) and methanol (Aldrich) were distilled over $CaCl_2$ and $Mg(OCH_3)_2$, respectively, shortly before use. NaH (Fluka, 65% oil dispersion), *p*-methoxyacetophenone (Aldrich, 99%), $NaOCH_3$ (Fluka, 30% solution in methanol), Hdbm (Aldrich, 98%), $FeCl_3$ (Carlo Erba, 99%), $NaClO_4 \cdot H_2O$ (Carlo Erba, 99.8%), and chloroform were used as received. A standard procedure was followed for the preparation of *p*-methoxymethylbenzoate from *p*-methoxybenzoic acid (Suchardt, 95%).

Hpmdbm [8]: In a 500 mL three-necked round-bottomed flask fitted with a dropping funnel and a condenser, NaH (7.81 g, 325 mmol) was added under dinitrogen to a stirred solution of *p*-methoxymethylbenzoate (8.309 g, 50 mmol) in anhydrous DME (120 mL). The mixture was refluxed for 30 min, then *p*-methoxyacetophenone (7.059 g, 50 mmol) was added dropwise, the reaction being monitored by TLC. After three hours the reaction mixture was cooled to room temperature and ice slowly added. The mixture was acidified with HCl 10% to pH 3, poured into water and extracted with diethylether (3 × 125 mL). The organic layers were then washed with water, dried over Na_2SO_4 and concentrated. The product was purified by recrystallization from *n*-hexane (yield: 75%). M.p. 112–113 °C; ^{1}H NMR (400 MHz, $CDCl_3$, 25 °C, TMS): $\delta = 3.88$ (s, 6H; OCH_3), 6.72 (s, 1H; =CH), 7.96 (d, ^3J(H,H) = 9.155 Hz, 4H; arom), 6.97 (d, ^3J(H,H) = 9.150 Hz, 4H; arom), 17.08 (s, 1H; enolic OH); $C_{17}H_{16}O_4$ (284.3): calcd C 71.82, H 5.67; found C 71.60, H 5.70.

$[NaFe_6(OCH_3)_{12}(dbm)_6]Cl \cdot CHCl_3 \cdot 12\,CH_3OH$ ($[1](Cl) \cdot CHCl_3 \cdot 12\,CH_3OH$): Sodium methylate (40 mmol) was added to Hdbm (2.243 g, 10 mmol) in anhydrous methanol (150 mL). The resulting solution was added, dropwise and under vigorous stirring, to a solution of resublimed ferric chloride (1.622 g, 10 mmol) in anhydrous methanol (30 mL). After 30 min stirring, the orange-yellow precipitate was filtered off, washed with methanol and dried under vacuum. 0.9 g of the above precipitate was suspended in 40 mL of a 1:1 chloroform:methanol mixture. Chloroform was added with stirring until complete dissolution. After 10 min stirring, the solution was filtered again and allowed to stand in air at room temperature. By slow evaporation of the solvent, large orange-red prisms of $[1](Cl) \cdot CHCl_3 \cdot 12\,CH_3OH$ formed in 7–10 days. The crystals were separated by filtration and dried under vacuum (10 mmHg, 4 h) (30% yield relative to the crude precipitate). IR (Nujol): $\tilde{\nu} = 3280$ (br), 1590 (s), 1530 (s), 1515 (s), 1305 (s), 1220 (m), 1065 (m), 1015 (s), 935 (w), 745 (s), 710 (m), 675 (m), 610 (w), 450 cm^{-1} (s); UV/Vis (1.6×10^{-5} M in $CHCl_3$): $\lambda = 255$, 275, 308, 403, 482 nm; $C_{103}H_{103}Fe_6O_{24}NaCl_4$ ($[1](Cl) \cdot CHCl_3$, 2224.8): calcd C 55.61, H 4.67, Fe 15.06, Na 1.03, Cl 6.37; found C 55.39, H 4.74, Fe 14.9, Na 1.2, Cl 7.1.

$[NaFe_6(OCH_3)_{12}(pmdbm)_6]ClO_4 \cdot x\,CHCl_3 \cdot y\,CH_3OH$
($[2](ClO_4) \cdot x\,CHCl_3 \cdot y\,CH_3OH$): The synthesis is analogous to that described above. Recrystallization was carried out in the presence of an excess of sodium perchlorate. Large deep-red prisms of $[2](ClO_4) \cdot x\,CHCl_3 \cdot y\,CH_3OH$ were separated by filtration and dried under vacuum (10 mmHg, 4 h). The yield relative to the crude precipitate is 95%. UV/Vis (1.2×10^{-5} M in $CHCl_3$): $\lambda = 499$, 405, 355, 329 nm; $C_{114}H_{126}Fe_6O_{40}NaCl$ ($[2](ClO_4)$, 2529.8): calcd C 54.13, H 5.02, Cl 1.40; found: C 54.45, H 4.90, Cl 1.5; the presence of sodium was confirmed by flame spectroscopy, and the possible occurrence of chlorides as counterions was excluded by potentiometric titration with $AgNO_3$ in an acetone/water solvent mixture.

Crystallography: A well-shaped individual crystal of $[2](ClO_4) \cdot x\,CHCl_3 \cdot y\,CH_3OH$ ($0.6 \times 0.5 \times 0.5$ mm) was sealed in a glass capillary containing a small amount of mother liquor. The data collection was performed at room temperature with a Siemens P4/RA rotating-anode diffractometer. Selected experimental parameters are presented in Table 1. Cell constants were calculated by least-squares fitting to the setting angles of 33 intense low-angle reflections ($16.3 < \theta < 27.8$). Laue group $\bar{3}$ was confirmed by automatic statistical analysis of the intensities of sample reflections. (*hkl*) reflections such that $-h + k + l = 3m$ for odd *m* were systematically absent, pointing to an *R* lattice. The intensity of standard reflections [(11 −5 7), (14 −9 5), (15 −4 1)] showed no appreciable decay during data collection. Lorentz polarization correction, but no absorption correction, was applied to collected intensities. The structure was solved by direct methods (SIR 92 [28]), which revealed the positions of all non-hydrogen atoms. Refinement was successfully carried out in space group $R\bar{3}$ with the SHELX76 program package [29]. Two rather intense electron density peaks outside the hexairon moiety (Cl_a and Cl_b) were refined as Cl atoms with fractional site occupancy factors (S. O. F.'s). All non-hydrogen atoms were treated anisotropically. Hydrogen atoms were assigned calculated positions with carbon–hydrogen distances constrained to 0.95 Å. A unique isotropic thermal parameter was refined for all hydrogen atoms. The final difference Fourier map was rather flat, the largest unaccounted-for peak being located near Cl_b (0.86 e Å^{-3}).

Crystallographic data (excluding structure factors) for the structure reported in this paper have been deposited with the Cambridge Crystallographic Data Centre as supplementary publication no. CCDC-1220-26. Copies of the data can be obtained free of charge on application to The Director, CCDC, 12 Union Road, Cambridge CB2 1EZ, UK (Fax: Int. code +(1223)336-033; e-mail: teched@chemcrys.cam.ac.uk).

Magnetic susceptibility and high-field magnetization measurements: Powder susceptibility measurements at 1 T were performed with a Métronique Ingéniérie SQUID susceptometer. 80 and 92 data points were collected in the temperature range 2.3–280 K from vacuum-dried 0.0355 and 0.0175 g samples of $[1](Cl) \cdot CHCl_3 \cdot 12\,CH_3OH$ and $[2](ClO_4) \cdot x\,CHCl_3 \cdot y\,CH_3OH$, respectively. Single-crystal measurements at 1 T were made with the same apparatus on an array of 3–4 large crystals of $[2](ClO_4) \cdot x\,CHCl_3 \cdot y\,CH_3OH$, which were carefully aligned under an optical stereomicroscope. 50 and 51 data points were collected in the ranges 2.2–100 and 2.2–150 K with $\boldsymbol{B} \perp \bar{3}$ and $\boldsymbol{B} \parallel \bar{3}$, respectively. The weight of the sample was determined by comparing the high-temperature average with powder data. All data were corrected for the magnetism of the sample holder, which was determined separately in the same temperature range and field, and for diamagnetic molecular contributions, which were estimated from Pascal's constants.

High-field DC magnetization data at 1.5 and 0.7 K for fields up to 20 T were collected by a vibrating sample magnetometer, modified for operation in the high-power water-cooled magnets of the Francis Bitter National Magnet Laboratory. A 0.0118 g powdered sample of $[1](Cl) \cdot CHCl_3 \cdot 12\,CH_3OH$ was encapsulated in a thin-walled Delrin container. Pulsed-field differential magnetization data were collected at 1.5 K for fields up to 52 T [11]. The magnet is the same as that described in ref. [30], but operating with a half-period pulse of 7.3 ms.

^{23}Na NMR spectra: ^{23}Na NMR spectra were recorded with a Bruker AMX-400 spectrometer operating at 105.85 MHz. $[1](Cl) \cdot CHCl_3 \cdot 12\,CH_3OH$ (0.015 g) was dissolved in 0.5 mL of $CDCl_3$ and the solution was transferred into a sodium-free quartz tube. The ^{23}Na chemical shifts (δ) were referenced to external NaCl (saturated solution in $CDCl_3$). Acquisition parameters: spectral width = 900 ppm, fid resolution = 2 Hz, relaxation delay = 0.1 s, no. of scans = 8 k. Left shifts of 8 data points and an enhancement function (LB = 100 Hz) were applied before the Fourier transform.

Acknowledgments: Thanks are due to E. McNiff, Jr., of the Francis Bitter National Magnet Laboratory for assistance in obtaining the 0–20 T magnetization data, to D. P. Goldberg for the local handling of the sample, and to S. J. Lippard for helpful discussion. We also acknowledge the Centro Interdipartimentale di Calcolo Automatico e Informatica Applicata (CICAIA) of Modena University for computer facilities, and the staff of the Centro Interdipartimentale Grandi Strumenti (CIGS) of Modena University for assistance during X-ray data collection. The work at the FBNML was supported by the National Science Foundation.

Received: April 1, 1996 [F342]

[1] a) *Biomineralization: Chemical and Biochemical Perspectives* (Eds.: S. Mann, J. Webb, R. J. P. Williams), VCH, New York, **1988**; b) K. S. Hagen, *Angew. Chem.* **1992**, *104*, 1036; *Angew. Chem. Int. Ed. Engl.* **1992**, *31*, 1010; S. J. Lippard, *ibid.* **1988**, *100*, 353 and **1988**, *27*, 344; c) S. M. Gorun, S. J. Lippard, *Nature* **1986**, *319*, 666.

[2] a) R. H. Holm, S. Ciurli, J. A. Wiegel, *Prog. Inorg. Chem.* **1990**, *38*, 1; b) G. Christou, *Acc. Chem. Res.* **1989**, *22*, 328.

[3] a) D. Gatteschi, A. Caneschi, A. Cornia, R. Sessoli, *Chem. Soc. Rev.* **1996**, 401; b) A. L. Barra, A. Caneschi, D. Gatteschi, R. Sessoli, *J. Am. Chem. Soc.* **1995**, *117*, 8855; c) R. Sessoli, D. Gatteschi, A. Caneschi, M. A. Novak, *Nature* **1993**, *365*, 141; d) D. P. Goldberg, A. Caneschi, R. Sessoli, C. D. Delfs, S. J. Lippard, *J. Am. Chem. Soc.* **1995**, *117*, 5789.

[4] A. Bencini, D. Gatteschi, *EPR of Exchange-Coupled Systems*, Springer, Berlin, **1990**.

[5] A. Caneschi, A. Cornia, A. C. Fabretti, D. Gatteschi, R. Sessoli, ■unpublished results.

[6] A. Caneschi, A. Cornia, A. C. Fabretti, D. Gatteschi, W. Malavasi, *Inorg. Chem.* **1995**, *34*, 4660.

[7] A. Caneschi, A. Cornia, A. C. Fabretti, D. Gatteschi, *Angew. Chem.* **1995**, *107*, 2862; *Angew. Chem. Int. Ed. Engl.* **1995**, *34*, 2716.

[8] Abbreviations used in the text: Hacac = 2,4-pentanedione; Hdbm = 1,3-diphenyl-1,3-propanedione; Hpmdbm = 1,3-di(*p*-methoxyphenyl)-1,3-propanedione; Hdpm = 2,2,6,6-tetramethyl-3,5-heptanedione; H_2sor = sorbitol; ami = zwitterion of β-alanine; phen = 1,10-phenanthroline.

[9] A. Caneschi, A. Cornia, S. J. Lippard, *Angew. Chem.* **1995**, *107*, 511; *Angew. Chem. Int. Ed. Engl.* **1995**, *34*, 467, and references cited therein.

[10] Recent ^{7}Li NMR experiments on $[LiFe_6(OCH_3)_{12}(dbm)_6]^+$ in chloroform solution have given analogous results.
[11] S. Foner, Y. Shapira, D. Heiman, P. Becla, R. Kershaw, K. Dwight, A. Wold, *Phys. Rev.* **1989**, *B39*, 11793.
[12] A. Trzeciak, T. Szymanska-Buzar, J. J. Ziolkowski, *Pol. J. Chem.* **1979**, *53*, 981, and references cited therein.
[13] K. L. Taft, C. D. Delfs, G. C. Papaefthymiou, S. Foner, D. Gatteschi, S. J. Lippard, *J. Am. Chem. Soc.* **1994**, *116*, 823.
[14] a) K. Hegetschweiler, H. W. Schmalle, H. M. Streit, V. Gramlich, H.-U. Hund, I. Erni, *Inorg. Chem.* **1992**, *31*, 1299; b) K. Hegetschweiler, H. W. Schmalle, H. M. Streit, W. Schneider, *Inorg. Chem.* **1990**, *29*, 3625; c) K. S. Hagen, V. S. Nair, *Inorg. Chem.* **1992**, *31*, 4048; d) K. L. Taft, G. C. Papaefthymiou, S. J. Lippard, *Science* **1993**, *259*, 1302; e) A. Caneschi, A. Cornia, D. Gatteschi, S. J. Lippard, G. C. Papaefthymiou, R. Sessoli, *Inorg. Chim. Acta* **1995**, *243*, 295.
[15] K. L. Taft, A. Caneschi, L. E. Pence, C. D. Delfs, G. C. Papaefthymiou, *J. Am. Chem. Soc.* **1993**, *115*, 11753.
[16] a) C. J. Brinker, G. W. Scherer, *Sol–Gel Science: The Physics and Chemistry of Sol–Gel Processing*, Academic Press, New York, **1990**; b) M. Guglielmi, G. Principi, *J. Non-Cryst. Solids* **1982**, *48*, 161.
[17] a) H. W. Rich, K. Hegetschweiler, H. M. Streit, I. Erni, W. Schneider, *Inorg. Chim. Acta* **1991**, *187*, 9; b) W. Schneider, *Chimia* **1988**, *42*, 9.
[18] a) M. S. Lah, V. L. Pecoraro, *Comments Inorg. Chem.* **1990**, *11*, 59; b) M. S. Lah, V. L. Pecoraro, *Inorg. Chem.* **1991**, *30*, 878.
[19] a) A. Cornia, A. C. Fabretti, D. Gatteschi, G. Pályi, E. Rentschler, O. I. Shchegolikhina, A. A. Zhdanov, *Inorg. Chem.* **1995**, *34*, 5383, and references cited therein; b) E. Rentschler, D. Gatteschi, A. Cornia, A. C. Fabretti, A. L. Barra, O. I. Shchegolikhina, A. A. Zhdanov, *Inorg. Chem.* **1996**, *35*, 4427.
[20] T. Tokii, K. Ide, M. Nakashima, M. Koikawa, *Chem. Lett.* **1994**, 441.
[21] A. K. Powell, S. L. Heath, D. Gatteschi, L. Pardi, R. Sessoli, G. Spina, F. Del Giallo, F. Pieralli, *J. Am. Chem. Soc.* **1995**, *117*, 2491.
[22] a) R. Orbach, *Phys. Rev.* **1958**, *112*, 309; b) T. de Neef, W. J. M. de Jonge, *Phys. Rev. B* **1975**, *11*, 4402; c) T. de Neef, *ibid.* **1976**, *13*, 4141; d) J. C. Bonner in *Magneto-Structural Correlations in Exchange-Coupled Systems* (Eds.: R. D. Willett, D. Gatteschi, O. Kahn), Reidel, Dordrecht, **1985**, p. 157.
[23] D. Gatteschi, L. Pardi, *Gazz. Chim. Ital.* **1993**, *123*, 231.
[24] a) S. J. Barclay, P. E. Riley, K. N. Raymond, *Inorg. Chem.* **1984**, *23*, 2005; b) B. Chiari, O. Piovesana, T. Tarantelli, P. F. Zanazzi, *ibid.* **1984**, *23*, 3398; c) S. Ménage, L. Que, Jr., *ibid.* **1990**, *29*, 4293; d) G. D. Fallon, A. Markiewicz, K. S. Murray, T. Quach, *J. Chem. Soc. Chem. Commun.* **1991**, 198.
[25] A. Cornia, D. Gatteschi, L. Pardi, unpublished results.
[26] M. Gerloch, J. Lewis, R. C. Slade, *J. Chem. Soc. A* **1969**, 1422.
[27] A. L. Barra, D. Gatteschi, P. Debrunner, C. S. Schulz, R. Sessoli, *Europhys. Lett.* **1996**, *35*, 133.
[28] A. Altomare, G. Cascarano, C. Giacovazzo, A. Guagliardi, *J. Appl. Crystallogr.* **1994**, *27*, 1045.
[29] G. M. Sheldrick, *SHELX76, Program for Crystal Structure Determination*, University of Cambridge, **1976**.
[30] S. Foner, *Appl. Phys. Lett.* **1986**, *49*, 982.
[31] *International Tables for X-ray Crystallography* (Ed.: T. Hahn), Reidel, Dordrecht (The Netherlands), **1983**.